12-2018

Use of stereolithographic 3D printing for fabrication of micro and millifluidic devices for undergraduate engineering studies

Cooper Thome
University of Tennessee at Chattanooga, gwf532@mocs.utc.edu

Follow this and additional works at: https://scholar.utc.edu/honors-theses

Recommended Citation

Use of Stereolithographic 3D Printing for Fabrication of Micro and Millifluidic Devices for Undergraduate Engineering Studies

Cooper Paul Thome

Departmental Honors Thesis

The University of Tennessee at Chattanooga

Department of Civil and Chemical Engineering

Examination Date: September 19, 2018

Bradley J. Harris, Ph.D.

Assistant Professor of
Civil and Chemical
Engineering

Thesis Director

Trevor Elliott, Ph.D.

Assistant Professor of
Mechanical Engineering

Department Examiner

ABSTRACT

Undergraduate STEM student performance is greatly benefited by supplementary, hands-on laboratory experience. Micro and millifluidic devices provide a multitude of opportunities for interactive study of concepts and phenomena encountered in nearly every field of engineering, as well as in chemistry, biology, and other disciplines. Unfortunately, due to the cost and difficulty of standard micro and millifluidic device fabrication methods, many undergraduate students do not have access to these versatile educational tools. Luckily, 3D printing offers an inexpensive and simple solution to this issue. This work aims to demonstrate the capability of stereolithographic (SLA) 3D printing for the fabrication of micro and millifluidic devices for use in undergraduate engineering studies at the University of Tennessee at Chattanooga (UTC); the ultimate goal of the work is to enhance student performance though the active study of concepts encountered in courses and undergraduate research projects. The work presented in this paper details the fabrication and analysis of various micro and millifluidic devices produced with a Formlabs Form1+ SLA printer, the initial results obtained through the use of the printed devices, and future plans for the continued integration of this technology into courses and undergraduate research at UTC. Initial experiments with these devices were intended to demonstrate 3D printing capabilities and potential utilization of the printed devices in studies and demonstrations related to fluid mixing, biodiesel production, and droplet generation. These applications were chosen for their relatability to topics covered in various engineering courses and potential for use in research at UTC.

TABLE OF CONTENTS

LIST OF FIGURES

LIST OF TABLES

CHAPTER 1: Scope of Work

1.1 Initial Focus

The initial focus of this work was centered on biodiesel production in microreactors using heterogeneous catalysis. The benefits of this system are that, as seen through previous studies, the micro-scale dramatically reduces the processing time and the heterogeneous catalysis does not create unwanted byproducts through saponification.[1,2] The cosolvent, a mixture of free fatty acids, is generally considered waste and contributes to unwanted products in standard homogeneous catalysis. However, with heterogeneous catalysis, the free fatty acid is converted directly to biodiesel. Past research suggests that the lattice structure of the heterogeneous catalyst may significantly affect the rate and extent of the reaction.[3,4] A very ordered, smooth catalyst may result in a varied reaction rate from that of an amorphous, rough catalyst. In this initial focus we intended to compare a highly ordered (200) nickel oxide lattice structure with an amorphous nickel oxide structure for catalytic efficacy. In addition to this, we intended to look at effects of residence time, mixing, heat transfer, and other factors to more fully understand, analyze, and optimize biodiesel production in microreactors using heterogeneous catalysis. The microreactors utilized in this study were to be fabricated at an outside facility. Unfortunately, the facility was unable to produce the desired microreactors due to complications in the fabrication process, and we were unable to fund further attempts to fabricate the devices.

1.2 Shift in Focus

After determining that the initial focus of biodiesel production in microreactors using heterogenous catalysis could not be pursued, we shifted our focus somewhat. In an effort to continue both previous work based on biodiesel production and work based on microfluidic use,

we sought other methods of microfluidic device fabrication. Ultimately, we determined that 3D printing held potential for inexpensive fabrication of microreactors intended for biodiesel production. However, since the deposition of a nickel oxide heterogenous catalysis is dependent on complicated and costly methods, we elected to use homogeneous catalysis for biodiesel production. We intended to provide a proof of concept for the use of stereolithography (SLA) 3D printed microreactors for continuous flow biodiesel production. In order to show efficacy of these devices, we planned to demonstrate resistance to heat, chemicals, and pressures associated with the reaction, in addition to analyzing the resultant biodiesel.

1.3 Expanded and Final Focus

As we worked to create devices for biodiesel production, we determined that the 3D printing of micro and millifluidic devices could have a wide range of applications at the University of Tennessee at Chattanooga (UTC). Instead of focusing strictly on biodiesel production, our final focus shifted and expanded to demonstrating proof-of-concept for the use of SLA 3D printing for the production of micro and millifluidic devices with various potential applications in education and research at UTC.

CHAPTER 2: Introduction

2.1 Undergraduate STEMEducation

Hands-on research and laboratory experience can greatly increase undergraduate STEM student success. For example, one large study performed at the University of Texas at Austin found that early engagement in course-based research significantly increased graduation rates for students with a broad range of sociodemographic characteristics.[5] An extensive review of studies focused on the benefits of undergraduate research experiences (UREs) found that students who do participate in undergraduate research typically have higher retention rates compared to their peers that did not participate in research. The review also concluded that URE participants hold the potential to increase student grades, confidence, and engagement in undergraduate STEM programs.[6] Multiple studies have also indicated that introducing hands-on laboratory experience can increase student's understanding, retention of material, and perceived success in a variety of areas.[7-9] Another extensive analysis of studies comparing traditional learning to active learning, such as hands-on experimentation, found that active learning can significantly increase student examination scores and decrease the likelihood of student failure in courses.[10] These studies and reviews thus support the use of hands-on experimentation and research for student success at the University of Tennessee at Chattanooga.

2.2 Micro and Millifluidics

Micro and millifluidic devices are devices containing channels or features with dimensions on the micro-scale or milli-scale, intended for the manipulation of fluid flow. Some researchers have classified the internal structures as *millifluidic* if over 1 mm, *sub-millifluidic* if in the 0.5–1.0 mm range, *large microfluidic* if in the 100–500 μm range, and *truly microfluidic* if

below 100 μm.[11] For simplicity, the term general term "micro and millifluidic" will be used to broadly refer to all of these classifications in this paper.

Micro and millifluidic devices have been used for research and undergraduate education in a variety of areas including pH sensing, particle separation, laminar flow, diffusive mixing, chemical synthesis, and droplet generation. These devices have typically been fabricated from a variety of materials using photolithography, soft lithography, and milling techniques; however, many of these fabrication processes are expensive or limited in their application[12,13] For example, photolithography can be used to produce small and precise features, yet is expensive and restricted to mostly 2-dimensional designs. Soft lithography is also expensive, as it requires the initial production of a template or mold, which is unfavorable during the development stages of a product where there may be many design iterations. Milling techniques are useful for design stages, but require very specific equipment, can experience a variety of issues, and are not fit for the fabrication of complicated 3D features.[14-16]

2.3 3D Printing of Micro and Millifluidic Devices

2.3.1 Overview

One form of microfluidic and millifluidic device fabrication that offers cheap, rapid production, along with the ability to produce more complex 3D features, is 3D printing.[14,15,17] Due to the increasing commercial availability of 3D printers, many researchers and educators are exploring the possibility of 3D printing microfluidic devices for a variety of applications.[18-20]

2.3.2 3D Printing Techniques

Both fused filament fabrication (FFF) and stereolithography (SLA), two of the most common 3D printing types, have been used for fabrication of microfluidic devices, but the viability of both printing types is dependent on the design and purpose of the devices being

produced. Both printing techniques are able to print models from an STL file format, created using 3D CAD software. In general, FFF involves the heating and extrusion of a thermoplastic material to fabricate 3D models in layers. Immediately after extrusion, the thermoplastic solidifies in place. FFF is by far the most widespread commercial 3D printing technique, and printers and materials are typically quite inexpensive. SLA is quite different from FFF in that, instead of a solid thermoplastic build material, the build material starts as a liquid photopolymer resin. In an inverted SLA setup (Figure 1), the photopolymer resin is contained in a clear resin tank. A build platform lowers into the resin and a laser cures the resin as specified by the 3D model. After one layer has been polymerized, the build platform rises and the next layer is cured.

Upside-Down (Inverted) SLA

1. Printed Part
2. Supports
3. Resin
4. Build Platform
5. UV Laser
6. Galvonometers
7. X-Y Scanning Mirror
8. Laser Beam
9. Resin Tank
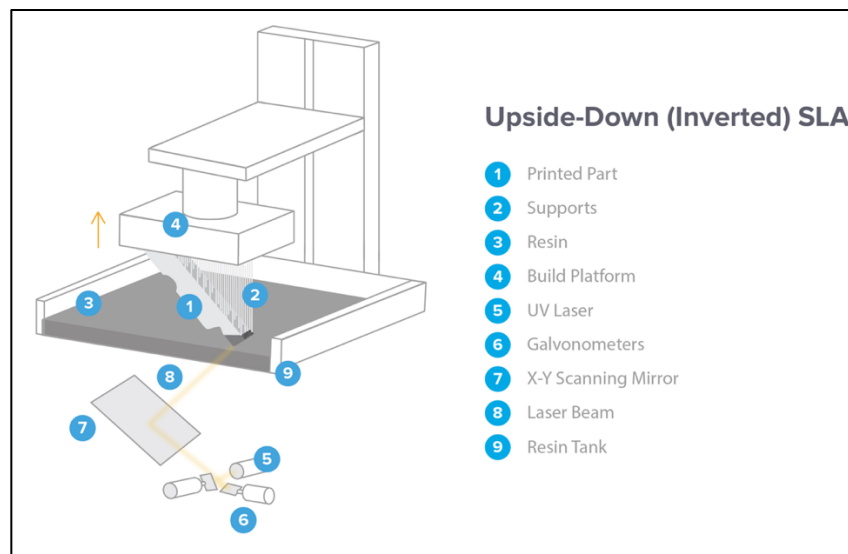
Figure 1. Inverted SLA printer schematic.[21]

SLA is typically capable of producing smooth, small channels, yet is limited to only UV curable resins or photopolymers as a printing material. FFF cannot typically produce channels as smooth or small as SLA, but is compatible with a wider range of printing materials.[11,17]

3.2.3 Device Design Approach and Issues

In general, there are two approaches to micro and millifluidic device fabrication when using 3D printing. In the first, channels and features are printed externally, such that the channels

14

are exposed and open; after printing, the channels and features can be enclosed in a variety of ways, including bonding a glass cover to the device or covering the device with polydimethylsiloxane (PDMS). While this approach can create working devices, it involves a sometimes complicated second fabrication step and, more importantly, severely restricts the ability to fabricate 3D structures within a device. The second approach is to print closed channels, which allows for fabrication of more complicated 3D features in a single step. The largest challenge that arises in this situation is the removal of uncured or sacrificial material left within the channels of the device. If channels are too small, it may be impossible to flush or remove this unwanted material. The minimum channel size that can be flushed is dependent on a variety of factors, including the printer and material used for fabrication, as well as the geometry of the channels and features themselves.[11] This study focused mainly on the direct fabrication of enclosed channels.

2.4 Explored Micro and Millifluidic Device Applications

2.4.1 Overview

In this study, devices were fabricated with the intent to demonstrate three main micro and millifluidic device applications: laminar flow and fluid mixing, biodiesel production, and droplet generation. These applications were chosen for their relatability to topics covered in various engineering courses, previous work conducted at UTC, and potential for use in future research at UTC.

2.4.2 Laminar Flow and Fluid Mixing

Due to low fluid flow velocity, hydraulic diameter, and viscosities normally seen in micro and millifluidic devices, fluids usually experience laminar flow within micro and millifluidic channels. This type of fluid flow is not often encountered or observed in everyday

life, and is distinct from turbulent flow, in which inertial forces play a large role in fluid mixing. The dimensionless Reynolds number, given by $Re = \rho uL/\mu$, where ρ is the fluid density, u is the mean velocity of the fluid, L is measurement of channel length, and μ is the dynamic viscosity of the fluid, is often used to compare the inertial and viscous forces within microfluidic devices. In micro and millifluidics, the Reynolds number is often below 1, and almost always well below 2000, indicating laminar flow of the fluids within the channels.[22] Thus, in laminar flow, fluid mixing is largely influenced by viscous forces and occurs mainly through diffusion, which is a slow process.[23,24] However, fluid mixing in micro and millifluidic devices can be encouraged through a variety of active and passive methods which increase the diffusion and chaotic advection of the fluids. Active methods for increasing mixing include use of oscillatory flow, microstirrers, or artificial cilia. Mixing can be encouraged passively by the addition of obstacles or grooves to the channels, by separating and recombining fluids by means of diverging and converging channels, as in lamination-based mixers, or by the introduction of mixing chambers, among other methods.[24-27]

In terms of education, the demonstration of laminar flow and diffusive mixing and the calculation and use of the Reynolds number, topics often discussed in fluid mechanics engineering courses, can be useful for undergraduate student understanding, as students are not typically exposed to such demonstrations in standard classes. Devices in which the mixing and flow of fluids can be easily manipulated and observed could thus be valuable tools for student understanding and retention of these topics. Furthermore, mixing of fluids within micro and millifluidic devices could be applied to many different areas of research at UTC.

2.4.3 Biodiesel Production

Previous researchers and manufacturers have used vegetable oil and methanol as a renewable feedstock to produce fatty acid methyl esters (FAME) or biodiesel through transesterification, shown in Figure 2, using homogeneous catalysts such as sodium hydroxide (NaOH) or potassium hydroxide (KOH) in batch processes. [3,28,29]
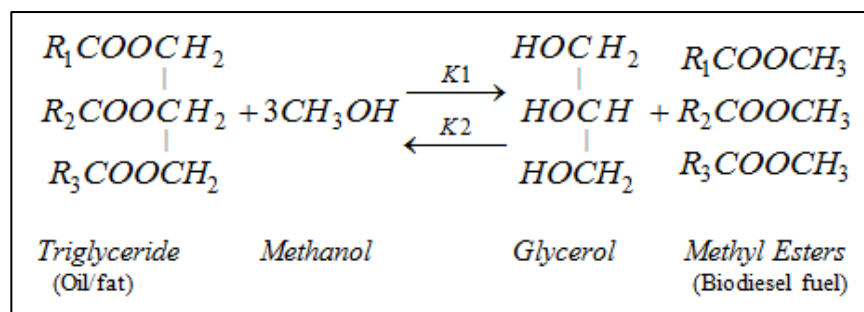
Figure 2. Overall transesterification reaction to produce biodiesel.[3]

However, the use of a batch process is often slow and inefficient compared continuous processing, which causes higher production costs. Some researches and educators have studied biodiesel production in microfluidic devices sometimes referred to as microreactors, and, in comparison to standard batch reactors, microfluidic devices are able to significantly reduce the processing time of biodiesel, per unit volume, from hours to minutes; this reduction in processing time is mainly attributed to the devices' high volume-to-surface area ratio and increased mass and heat transfer rate.[1,30] Compared to petroleum diesel, biodiesel produces less carbon monoxide, sulfur dioxide, and unburned hydrocarbons, and because of its similarity to petroleum diesel, it is a worthy alternative for use in many of the areas where petroleum is currently used, including transportation.[29]

Research into biodiesel production methods is highly applicable for chemical engineering students entering industry focused on alternative energy and fuels. The exploration of biodiesel production in microreactors could greatly increase student understanding of alternative energy, chemical synthesis, and general laboratory practices. Furthermore, comparison between standard

batch production of biodiesel and microfluidic production of biodiesel could help students expand and solidify knowledge obtained in standard chemical engineering courses, which typically focus on batch and plug flow reactors.

2.4.4 Droplet Generation

Microfluidics have also been used for droplet generation studies in education and research. Droplet in a continuous phase can be used to encapsulate cells or create emulsions, among other applications.[20,31] For example, one study used a FFF-fabricated droplet generator to encapsulate stem cells in alginate droplets in a continuous sunflower oil phase in order to determine viability of the stem cells.[32]

Because of the low Reynolds numbers typically seen in micro and millifluidic devices, in addition to very small Bond numbers, which compare gravitational forces to surface forces, and small Weber numbers, which compare inertial forces to surface forces, it can be assumed that inertial forces are dominated by interfacial and viscous forces within these devices. The Capillary number compares the interfacial forces and surface forces, and, at low capillary numbers, spherical droplets may be formed due to increased effects of interfacial tension. [22,33]

A variety of passive designs for droplet generation have been created, including devices based on T-junctions and flow focusing. Some researchers have even utilized active elements, such as adjustable orifices and electrodes, in order to produce droplets. In general, droplets are formed passively when two different phases meet and the interface of the phases is deformed, eventually leading to the break-off of a droplet within the continuous phase.[33] Droplet sizes produced by micro and millifluidic droplet generators can be influenced by a variety of factors including general device design and flow rate ratio, both of which can be easily studied and manipulated by students.[34]

The tuning of droplet size though manipulation of flow rate is easily relatable to chemical engineering courses in which understanding of fluid flow is essential. Furthermore, the ability to encapsulate cells could enhance current bioengineering research being conducted at UTC.

CHAPTER 3: 3D SLA Printing

3.1 Overview

All 3D printing in this study was performed using a commercial SLA 3D printer. The software, 3D printer and materials, 3D printing post-cure process, and printing challenges are detailed here. Most models in this study were printed at a 50 micron resolution directly on the printer build platform.

3.2 3D Printer

A commercial Formlabs Form 1+ printer (Figure 3) was used for the fabrication of all devices and models in this study. The printer, which fits on a desktop, utilizes a 405nm violet laser to polymerize various liquid resins, and the layer thickness of prints can be set to 25, 50, or 100 microns, depending on the resin used.[35] The internal mechanisms and components of the printer are similar to those shown in Figure 1. Some of these components can be seen through the transparent orange cover, which prevents users from being exposed to the laser while also allowing for observation during the printing process.

Figure 3. Formlabs Form1+ printer.

Formlabs printers are commercially available for approximately $3500, which is relatively inexpensive compared to costs incurred during typical micro and millifluidic device design and fabrication.[37] As of 2018, the Formlabs Form1+ printer is being phased out and replaced by a newer version, the Formlabs Form 2. Formlabs still offers support and repairs for the Form 1+, and build plates and resin tanks the Form 1+ will be available for a limited amount of time, based on stock.[38] While these changes did not impact this study, any continued work will more than likely require upgrading to a Form 2 or similar 3D printer.

3.3 3D Modeling and Printing Software

3.3.1 AutoCAD

AutoCAD software was used for all modelling in this study. AutoCAD layers were used extensively so that device channels, ports, and bodies could be easily manipulated. Additionally, many models were designed such that modular connection of various devices was possible both virtually in AutoCAD software and physically after printing.

3.3.2 PreForm

Final designs were exported as STL files and imported into Formlabs' PreForm software which prepares STL files for printing with Formlabs printers. This software allows for selection of printed layer thickness, orientation of models, and adjustment of the z-offset of the printer build plate, among other options. In cases where models required supports for printing, the supports were generated using this software.

3.4 Photopolymer Resins

All photopolymer resins used in this study were purchased directly from Formlabs, which offers a variety of resins for various applications. The cost of these resins ranges from \$100 to \$200 per liter. Because of their reported thermal and chemical compatibility, both Formlabs High Temp Resin and Formlabs Clear resin were investigated and tested for fabrication of devices. Ultimately, devices were printed using Formlabs High Temp Resin.

3.4.1 Formlabs High Temp Resin

Formlabs High Temp resin produces prints that are relatively transparent, depending on the thickness of the print. Formlabs reports High Temp Resin to have a heat deflection temperature of 289°C at 0.45 MPa, which is well above temperatures encountered in any portion of this study. This thermal resistance is dependent on a post-cure treatment, detailed in section 3.5. Formlabs also provides a limited amount of solvent compatibility data, and reports High Temp prints experience less than 1% weight gain after 24 hours of exposure to diesel and 0.025% sodium hydroxide solution.[39]

3.4.2 Formlabs Clear Resin

Formlabs Clear resin produces prints which are somewhat more transparent than that of High Temp resin. Formlabs reports Clear Resin to have a heat deflection temperature of 73.1°C at 0.45 MPa, which is also above temperatures encountered in this study. Formlabs tests reported

Clear Resin to experience less than 1% weight gain after 24 hours of exposure to diesel and 0.025% sodium hydroxide solution.[40]

3.5 3D Printing Post-Treatment

After printing, all parts were agitated in isopropyl alcohol (IPA) for two minutes, followed by three minutes of undisturbed soaking in IPA. The parts were then transferred to another IPA bath, agitated for two minutes, and allowed to soak for three more minutes. For devices containing channels, pressurized air was used to force unpolymerized resin from the channels. After clearing the channel with pressurized air, IPA was pumped through the channels to remove any remaining unpolymerized resin. All parts were then post-cured for 30 minutes in a post-cure chamber (Figure 4). This chamber was constructed by wrapping a 16.4 foot strip of 395-405nm lights, purchased through Amazon.com, around the inside of a small bucket.

Figure 4. Post-cure chamber without cover.

Parts were situated inside the chamber such that they experienced light exposure from all directions to facilitate full curing. When preparing devices that would be exposed to elevated temperatures, the devices were subsequently placed in an oven at 60˚C for 30 minutes. When attaching devices in a modular fashion, ports were connected and unpolymerized resin was coated over seams. The unpolymerized resin was then irradiated by a 405 nm laser, purchased through Amazon.com, effectively polymerizing the resin and bonding the devices. This technique was also used to patch holes or correct other issues in some defective prints.

3.6 3D Printing Challenges

3.6.1. General

A variety of issues with the 3D printing process arose over the course of this study. Some of these issues include detachment of models from the build platform during printing and over curing of resin within channels. The latter issue was investigated through channel tests, detailed in Chapter 4 of this document. Overall, the largest 3D printing issue experienced during this study was clouding of the resin tank, which only occurred when using High Temp resin.

3.6.2 Resin Tank Clouding

After repeated use of a single resin tank, the tank would begin to experience clouding, as shown in Figure 5. This clouding decreases the accuracy of the laser's focus and often leads to over polymerization of the resin, distorted prints, and regions of partially polymerized resin within the tank. Furthermore, resin often cured directly to the tank rather than the platform, leading to further clouding and damage to the tank.

Figure 5. Clouding in resin tank after repeated use.

When tanks experienced such clouding, replicability of prints was decreased and the ability to

print flushable channels became severely restricted. In these cases, the clouded tank and leftover

resin were replaced with a new resin tank containing fresh resin, restoring the ability to print

designs accurately and precisely. New tanks and resin typically lasted around 30 print cycles

before experiencing such clouding, depending on the number of models being printed at once.

The clouding was usually worse at points where multiple models had been printed. In order to

slow clouding, models were moved around the build platform to avoid excessive overlapping of

regions that had been printed on before.

CHAPTER 4: Channel Tests

4.1 Overview

The objective of the channel test study was to demonstrate and investigate the capability of the Formlabs 1+ printer to fabricate both covered and exposed micro and millifluidic channels. While direct printing of devices containing enclosed channels was the main objective of the overall study, printing and analysis of exposed channels both helps to understand the fabrication of closed channels and provides a basis for possible future work in which exposed printed channels are enclosed with a cover in a second fabrication step. Overall, the knowledge gained through this study was intended to inform subsequent design of micro and millifluidic devices for utilization at UTC and beyond.

4.2 Channel Test Design

Channel test pieces (Figure 6) consisted of a series of five channels of varied cross-sectional area in square, rectangular, and cylindrical geometries. Covered channel tests included a port for flushing of unpolymerized resin. The exposed channel test pieces were modeled using the channels from the covered channel tests, but with no top to the channel for the rectangular and square geometries. In the case of the cylindrical channels, only half of the channel was printed such that the cross section of the channel was a semicircle.
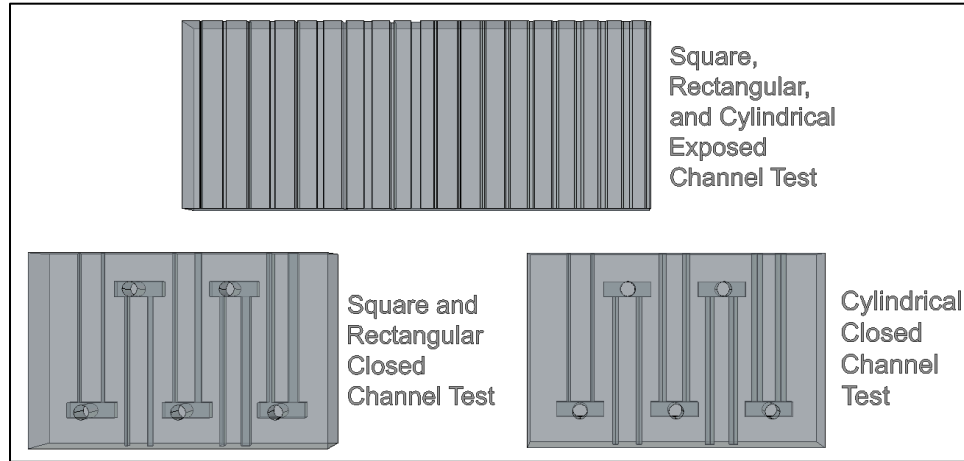
Figure 6. Models of all three channel test pieces.

The dimensions of the designed channels are shown in Table 1, below. Note that, while cross-sectional areas of the square and rectangular channels differ slightly from that of the cylindrical channels, the cross-sectional areas are reasonably comparable.

Table 1. Designed channel dimensions.

Square Channels				Rectangular Channels				Cylindrical Channels		
Channel	Height (μm)	Width (μm)	Cross Sectional Area (μm^2)	Channel	Height (μm)	Width (μm)	Cross Sectional Area (μm^2)	Channel	Radius (μm)	Cross Sectional Area (μm^2)
Square 1	1050	1050	1102500	Rectangle 1	2100	525	1102500	Cylinder 1	600	1130973
Square 2	900	900	810000	Rectangle 2	1800	450	810000	Cylinder 2	500	785398
Square 3	700	700	490000	Rectangle 3	1500	350	525000	Cylinder 3	400	502655
Square 4	550	559	307450	Rectangle 4	1100	275	302500	Cylinder 4	300	282743
Square 5	350	350	122500	Rectangle 5	700	175	122500	Cylinder 5	200	125664

4.3 Channel Test Analysis

Channel test pieces were printed directly on the build platform without supports at a 50 micron resolution. The resultant prints were analyzed using optical microscopy, and printed channel dimensions were compared to that of the AutoCAD design. In order to obtain multiple representative cross-sectional measurements, the printed channel test pieces were sanded

perpendicular to the channels. Five to seven cross-sectional images were taken and analyzed

using Micron imaging software over a 3mm length for all channel tests. The height, width, and

cross-sectional area of the exposed and closed square and rectangular channels were measured,

while the equivalent "height" and "width" diameters and cross-sectional areas were measured for

the exposed and closed cylindrical channels.

4.4 Channel Test Results and Discussion

All exposed channels were successfully printed aside from the smallest rectangular and

cylindrical channels which contained some regions of over cured resin. The largest four sizes of

cylindrical channels, four sizes of rectangular channels, and two sizes of square channels were

successfully flushed in the closed channel test pieces (Figure 7).
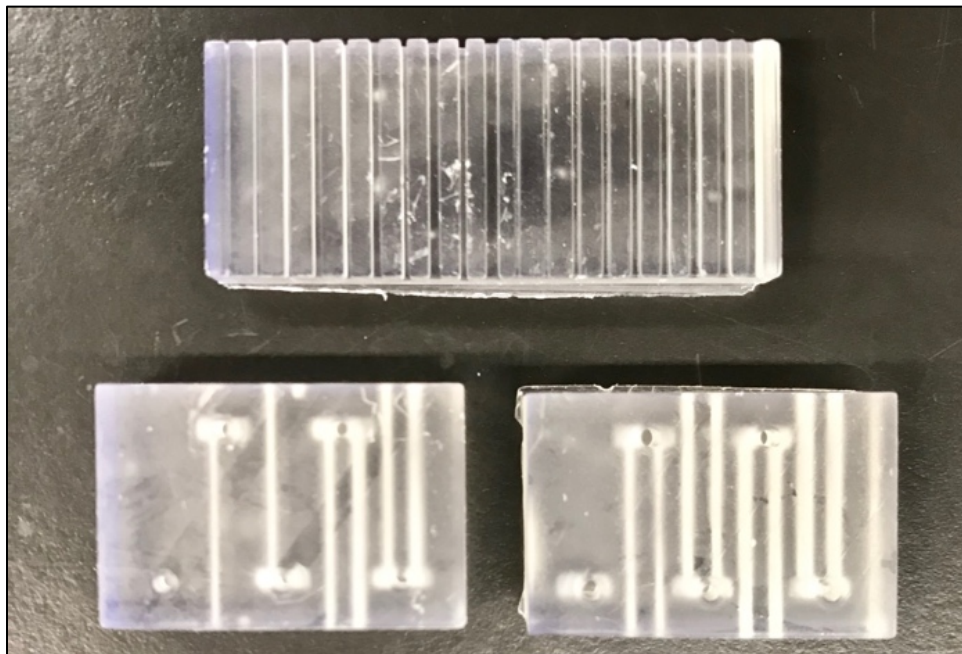
Figure 7. Printed channel test pieces.

Cross sectional dimensions were measured for all channels that were successfully printed.

Examples of cross sectional views of printed channels designed to have an equivalent cross

sectional areas of around 80,000 μm^2 (Square 2, Rectangle 2, and Cylinder 2 from Table 1) are

shown in Figure 8. The fragmented portion on the left side of the rectangular channel shown in Figure 8 is due to the sanding process employed to sample cross sections of the channels and is not a result of any part of the printing process. Overall, the channel sidewalls are appeared to be quite uniform and smooth, but quantification of the roughness of channels may be of interest during future studies.
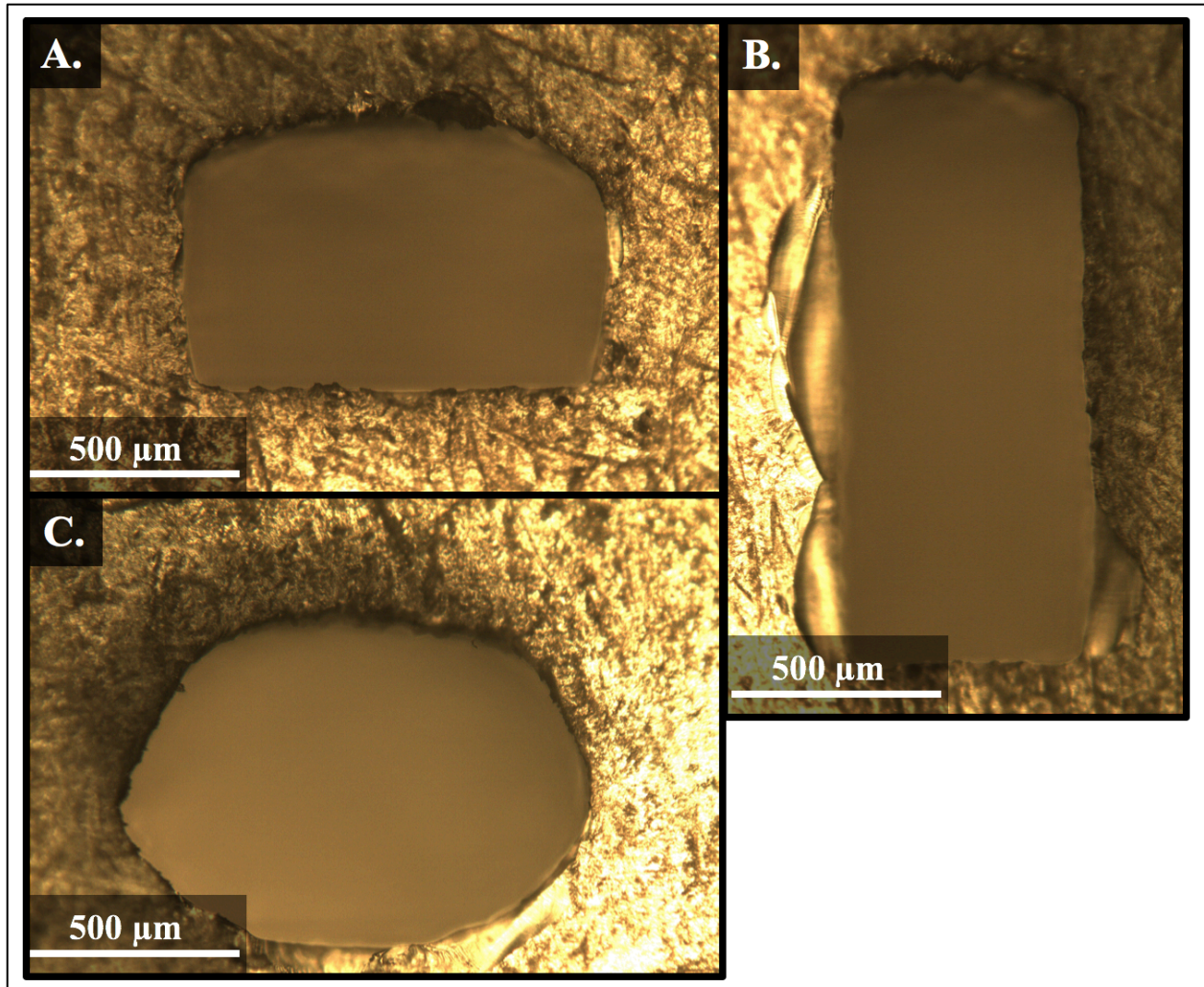
Figure 8. (A) Images of square, (B) rectangular, and (C) cylindrical cross sections. Measured square, rectangular, and cylindrical channel heights are shown in Figure 9, Figure 10, and Figure 11, respectively. Measured square, rectangular, and cylindrical channel widths are shown in Figure 12, Figure 13, and Figure 14, respectively. Measured square, rectangular, and

cylindrical channel cross-sectional areas are shown in Figure 15, Figure 16, and Figure 17, respectively. Note that channels that could not be flushed are not included in these figures.
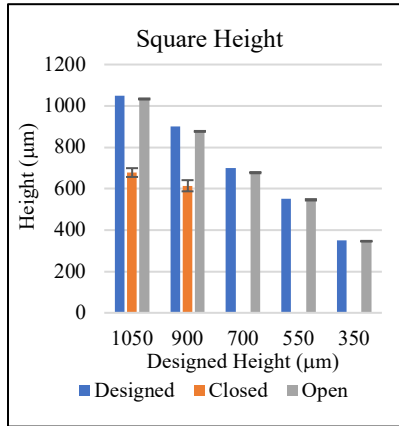
Figure 9. Square channel heights.
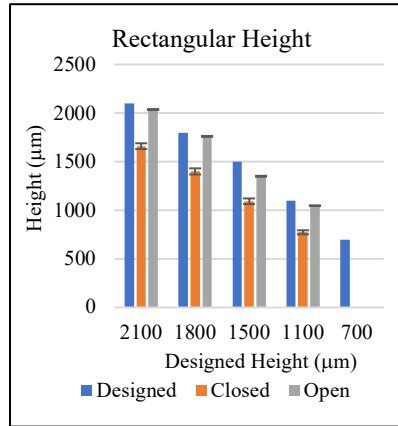
Figure 10. Rectangular channel heights.
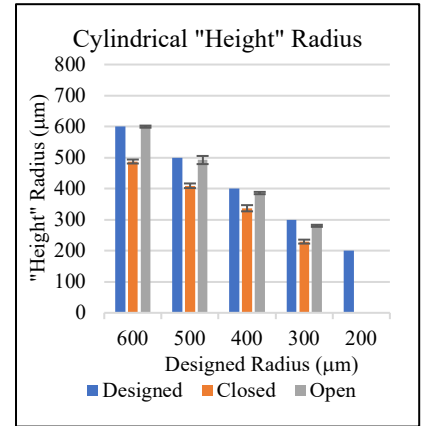
Figure 11. Cylindrical channel "height" radii.
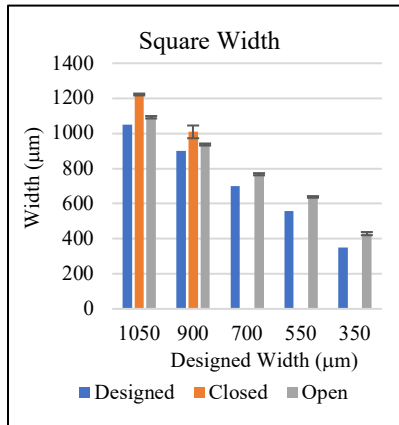
Figure 12. Square channel widths.
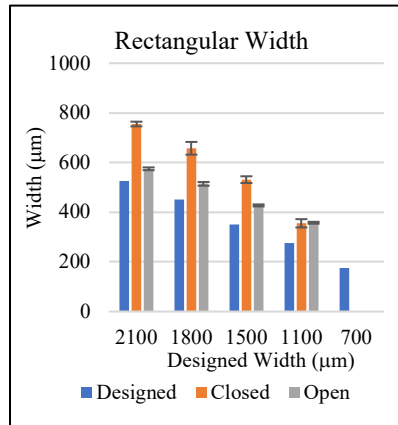
Figure 13. Rectangular channel widths.
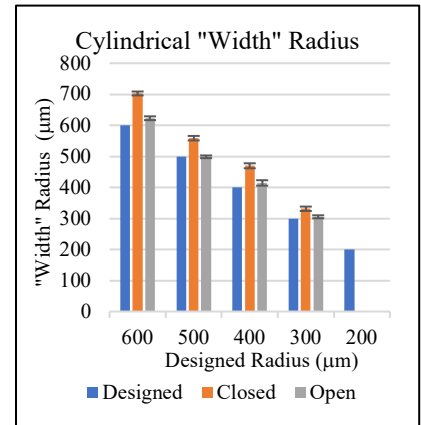
Figure 14. Cylindrical channel "width" radii.
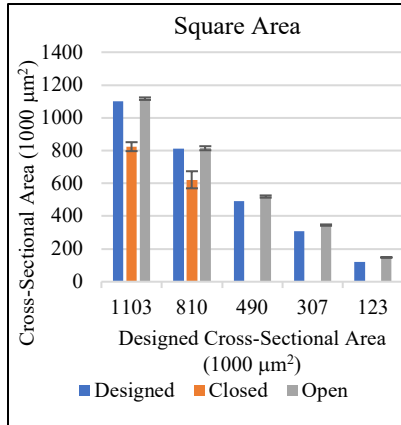
Figure 15. Square channel cross-sectional areas.
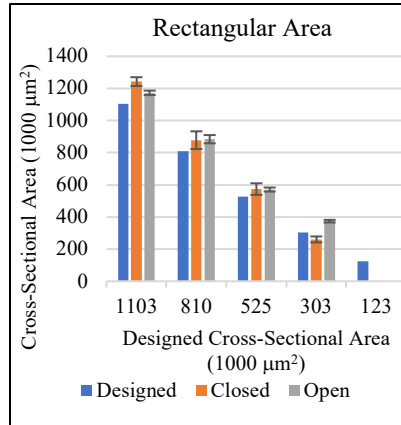
Figure 16. Rectangular channel cross-sectional areas.
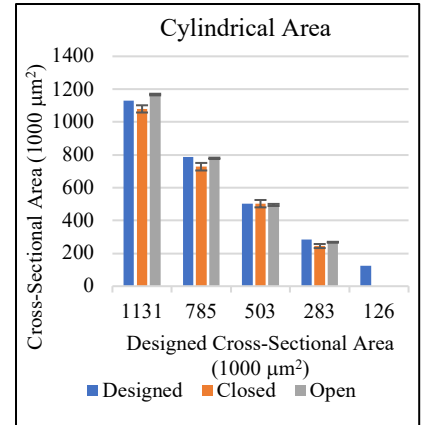
Figure 17. Cylindrical channel cross-sectional areas.

For all geometries of closed channels, the heights of the channels were consistently less than the designed height, while the width was consistently larger than that of the designed width. Overall, the cross-sectional area of the closed cylindrical channels most closely aligned with that of the design, though the cross section was elliptical rather than circular. Open channel dimensions much more closely aligned with that of the design, leading to the conclusion that, by closing the channel, over curing of resin within the channels occurs. If future work utilizes open, exposed channels, these results may be helpful as they indicate that open channel dimensions more closely agree with designed dimensions. However, this remainder of this work focuses only on closed channels; because closed cylindrical channels most closely agreed with designed dimensions, experienced less variance, and were able to be properly flushed over a larger range of cross-sectional areas compared to the square channels, cylindrical channels were mostly used for later design of micro and millifluidic devices.

31

CHAPTER 5: Laminar Flow and Fluid Mixing

5.1 Overview

The first device application demonstrated in this study was fluid mixing. Initially, a device with a straight, unobstructed, cylindrical channel was designed and printed to demonstrate laminar flow. After this, multiple devices were designed with the intent to demonstrate fluid mixing and diffusion. The device designs, mixing demonstration methods, demonstration results, and plans for future work are reviewed here.

5.2 Device Design

5.2.1 General

Most devices in this study had a few similarities. Firstly, the main internal channels of devices were typically modelled as cylinders with radii of 0.4 to 0.6 mm, as this channel design lead to successful and reproducible device fabrication. Secondly, many devices were designed with the same type of port which can allow for modular connection of devices, if desired. These ports have a "female" and "male" component, as seen in Figure 18. In cases where devices were used for multiple experiments with various fluids, tubing was lightly scored and was subsequently inserted and bonded to the male port component by applying unpolymerized printer resin to the interface of the tube and male component and curing the resin with a 405nm laser. The tubing connected to the male port component could then be attached to a syringe. After this, small gaskets were placed between the male and female components to prevent leaking, and the male component was snapped into the female component. In cases where the two components did not fit properly or form a sufficient seal, the male and female port interface was coated with uncured resin which was then cured, forming a water-tight seal. In some cases, the male port

component was not needed, and the tubing was inserted directly into the cylinder in the female port component. If necessary, this tubing and port interface was joined by directly curing resin over the area.
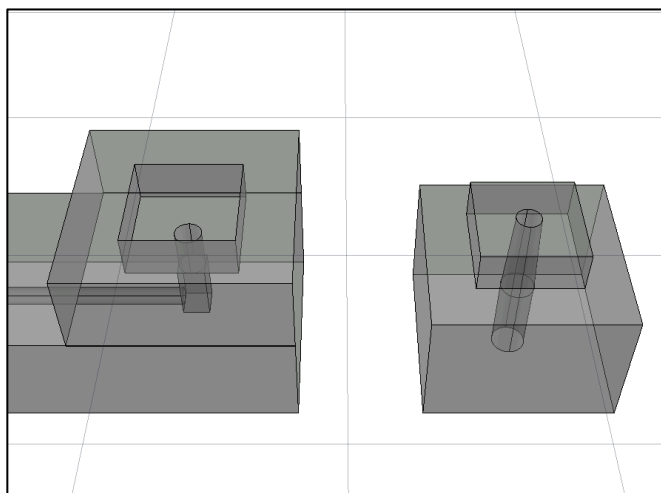
Figure 18. Models of female port component on laminar flow device (left) and male port component (right).

5.2.2 Various Designs

Figure 19 shows a variety of device models that were printed and tested to either show laminar flow (Device A), or fluid mixing (Devices B,C,and D).

A. B. C. D.
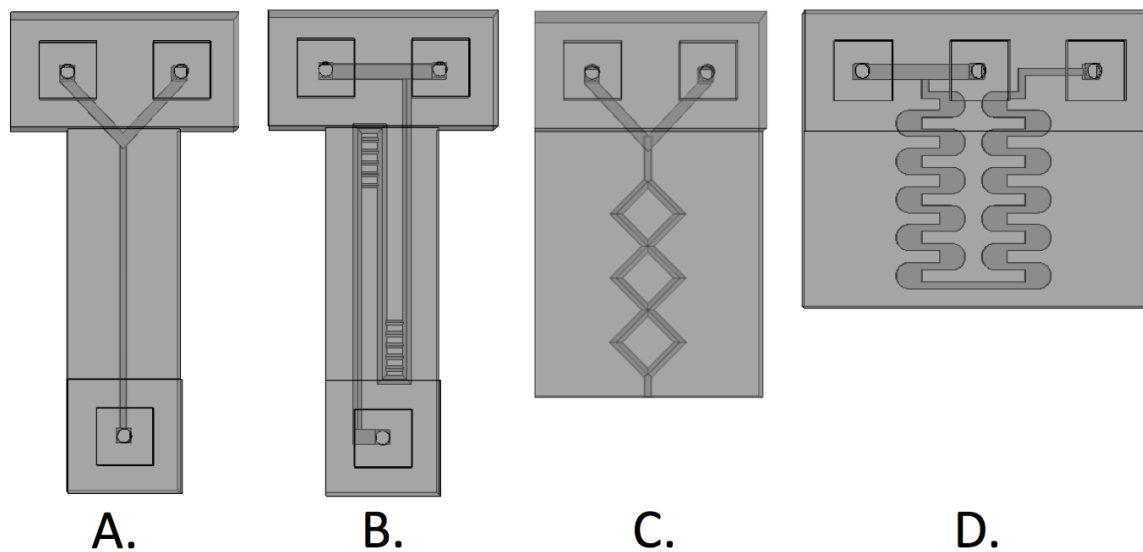
Figure 19. Models of (A.) Laminar flow device, (B.) Lamination-based mixing device, (C.) Divergence/convergence mixing device, and (D.) Chamber mixing device.

Device A contained a single, 0.5mm designed radius channel with no obstructions. Device B contained a main channel with a designed radius of 0.5mm, as well as multiple smaller channels with designed radii of 0.3mm. These smaller channels were intended to separate flow to encourage mixing through lamination of the flow which increases the contact surface area between two fluids. Device C also contained channels with designed radii of 0.5mm which diverge and converge to encourage splitting and recombination of fluids, thus increasing mixing. Device D included multiple chambers with a height of 1.15mm, which were intended to increase mixing in a manner similar that demonstrated in circular chambers by Alam and Kim.[41] Figure 20 highlights three modular devices designed for fluid mixing encouraged by internal obstructions.
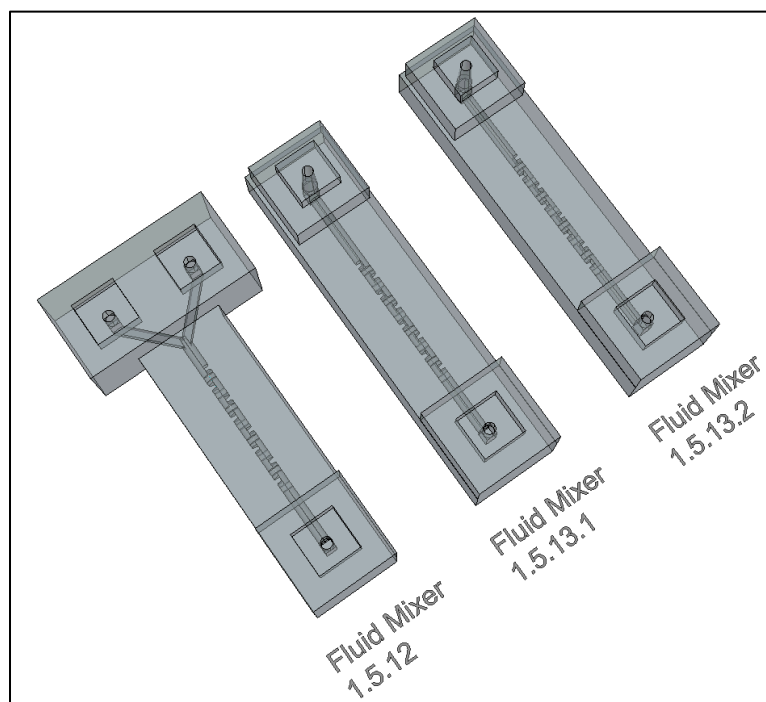
Figure 20. Models of various modular fluid mixers.

All three devices contain obstructions covering half of the cylindrical channel, which had a designed radius of 0.5mm. Each obstruction was rotated 90 degrees relative to the last

obstruction to create a spiraling baffle effect (Figure 21) in order to encourage fluid mixing and diffusion.
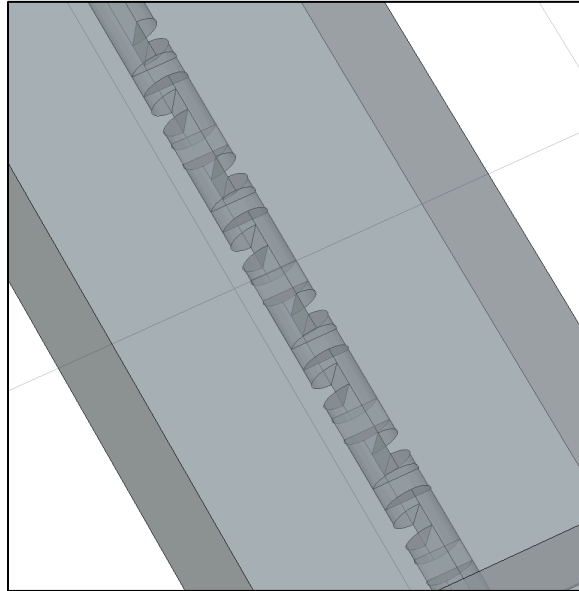
Figure 21. Close up of channel with spiraling baffles rotated clockwise relative to flow of liquid. The obstructions of the middle device in Figure 20 were rotated counterclockwise relative to the direction of flow, as opposed to clockwise as in the other two devices, which theoretically promotes rotation and mixing of fluid in opposite directions. When physically connected in series, a long channel with the desired mixing effect is created.

5.3 Mixing Demonstration Methods

Water colored with blue and red commercial food coloring was used for all demonstrations of fluid flow and mixing, which was observed visually. A Cole Parmer KDS Legato 210 syringe pump was used to pump fluids through the various devices at a rate of 2ml/hour. Fluorinated ethylene propylene (FEP) tubing with an outer diameter of 1/16 inches and inner diameter of 0.020 inches was used to connect syringes and devices.

5.4 Laminar Flow and Fluid Mixing Results and Discussion

5.4.1 Laminar Flow Device Demonstration

A printed device containing a straight cylindrical channel of designed radius 0.5 mm can be seen in Figure 22. Two different colored water solutions enter the ports on the left of the device, and no significant mixing of the two fluids is apparent throughout the channel. This device provides an excellent visual representation of laminar fluid flow with limited diffusive mixing.
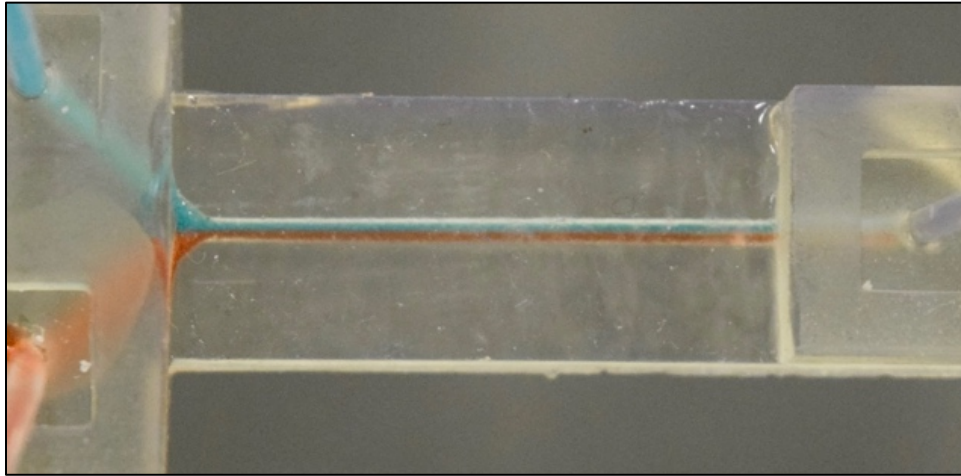
Figure 22. Printed device with straight cylindrical channel of radius 0.5 mm.

5.4.2 Mixing Devices

Figure 23 shows a printed device similar to Device B in Figure 19, intended for lamination-based mixing. As seen below, the fluid flow is still laminar and the fluids do not appear significantly mixed as they exit the device on the right. In fact, the flow reached a steady state in which the two liquids traveled through a specific path and appeared to remain in laminar flow. For example, the top right portion of the channel with the three cross channels was intended to separate portions of the red fluid and introduce them back to the main channel flow at different points. However, as observed, the red fluid simply traveled through the first cross channel. This is more than likely a result of the cross channels being too large in diameter to create the desired flow pattern and effect at a flow rate of 2ml/hr. This behavior was also noted at flow rates up to

8ml/hr. Unfortunately, channels smaller than the cross channels in this devices could not be produced and flushed consistently.
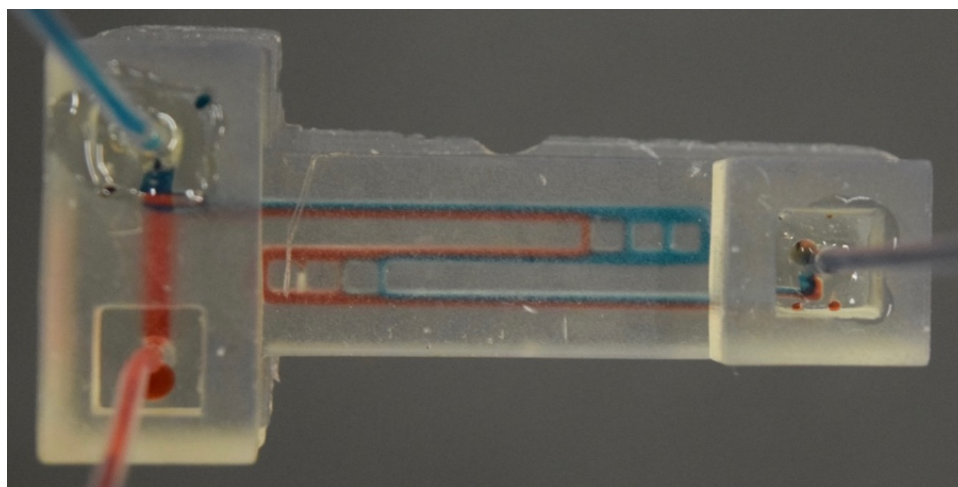
Figure 23. Lamination-based mixing device during experiment.

Figure 24 shows a printed model of Device C from Figure 19, which was intended to encourage mixing through separation and recombination of streams. As in the lamination-based mixing device, fluids traveled through specific paths and did not mix extensively. Again, it is speculated that this is due to channels being too large in diameter.
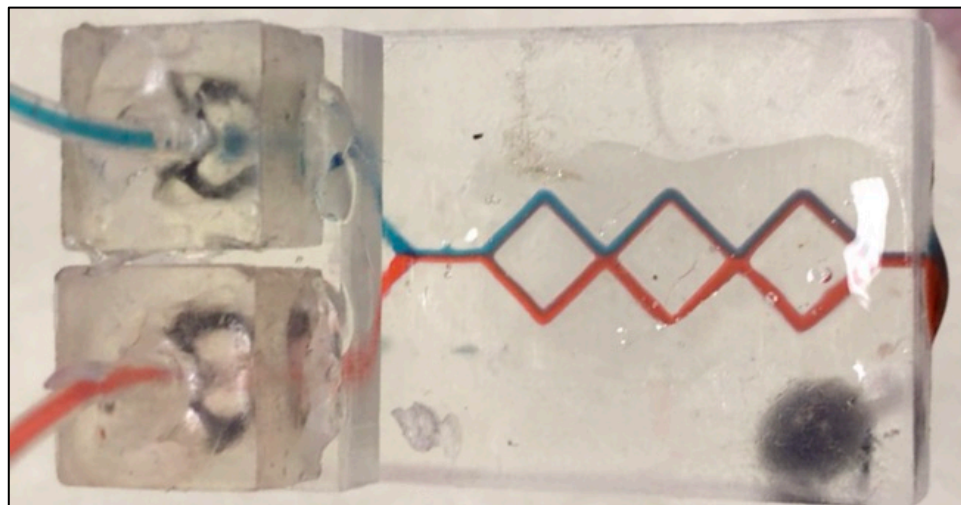
Figure 24. Divergence/Convergence mixing device printed with Clear Resin during experiment.

Figure 25 shows a printed model of Device D from Figure 19, which was intended to encourage mixing in chambers. As easily seen, the fluids remained in laminar flow and only slight diffusion

of fluids is noted at their interfaces. As with the previous mixing devices, we speculate that the

chambers and channels of this device are too large to encourage proper mixing in the chambers.
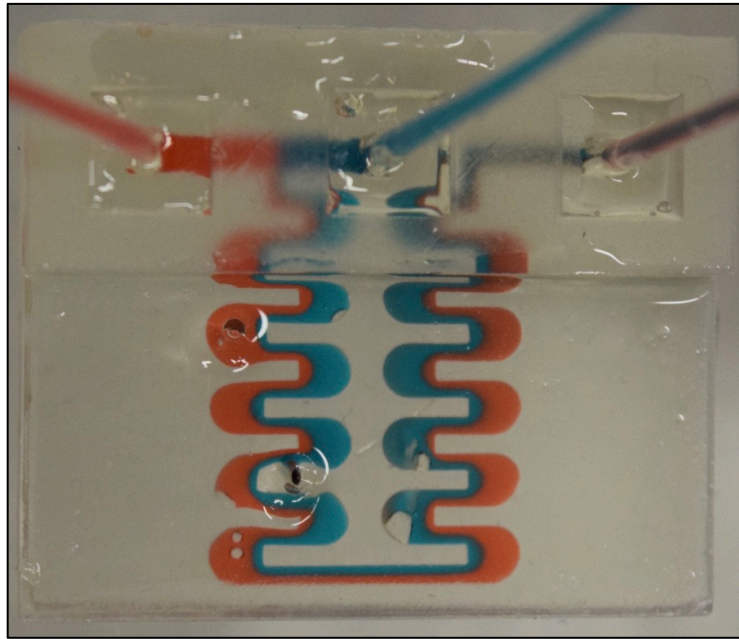
Figure 25. Chamber mixing device during experiment.

While the lamination-based, diverging/converging, and chamber mixing devices did not achieve

desired mixing effects, the designs may serve as a basis for future designs of devices intended

fluid mixing through similar methods. For example, if reduction of the scale of the channels and

chambers can be achieved in future 3D printing efforts, the devices may exhibit the desired

effects.

Figure 26 shows the modular devices designed for fluid mixing. In the first device

separate red and blue regions can be easily observed. As the fluid continues through the device,

the rotated baffles encourage mixing and diffusion, and, by the last device, the liquid appears to

be well-mixed and regions of blue and red water are not observed, as detailed in Figure 27.
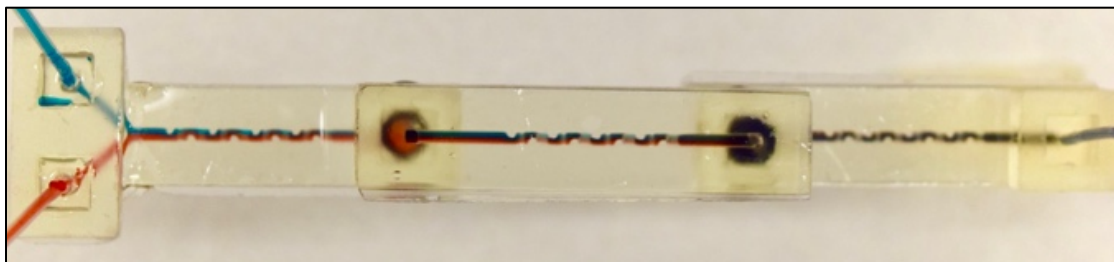
Figure 26. Connected devices during fluid mixing demonstration.
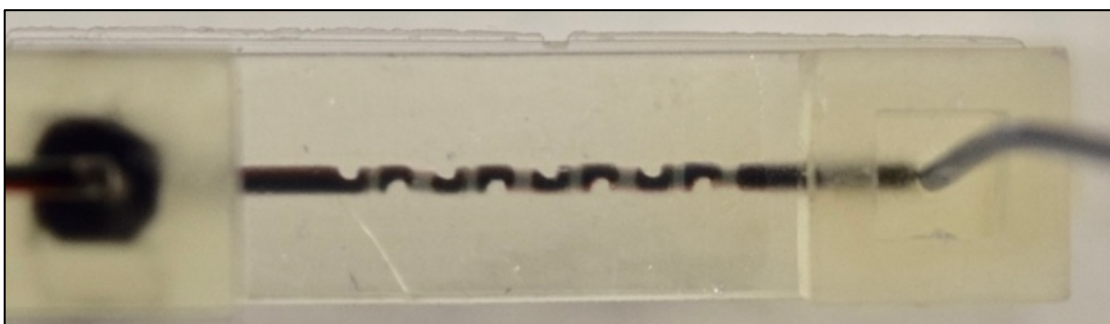
Figure 27. Close up of last section of device in **Figure 26**.

This modular device arrangement appeared to achieve successful fluid mixing. However, more conclusive measurement of mixing, in addition to further characterization and measurement of the printed devices, is encouraged for future work.

5.5 Future Work

Future work focused on quantitative measurement of mixing in devices is recommended. Some methods of quantitative mixing measurement include high resolution stereo micro particle image velocimetry and the use of acid-base indicator reactions.[42] The ability to make these measurements could greatly broaden the number of demonstrations and experiments that undergraduates could conduct. Furthermore, this data could inform future fluid mixer design, which should be the second major area of focus for these studies. Some examples of future work in this area include exploration into fabrication of other devices containing multiple channels or

more complicated 3D features for fluid mixing, in addition to the reduction of channel size

within devices similar to those printed in this study.

CHAPTER 6: Biodiesel Production

6.1 Overview

Before biodiesel product experiments were conducted, both High Temp and Clear resin underwent chemical resistance testing to determine compatibility with chemicals involved in the biodiesel transesterification reaction. After this, biodiesel was produced through a lab-scale batch reaction. Printed fluid mixing devices were then used in micro and millifluidic biodiesel production experiments.

6.2 Chemical Resistance Testing

6.2.1 Chemical Resistance Test Design

Chemical resistance testing was based ASTM D543.[42] First, disks with a designed radius of 50.80 mm and designed thickness of 3.217, shown in Figure 28, were printed in both High Temp and Clear resin and cured in the post-cure chamber.
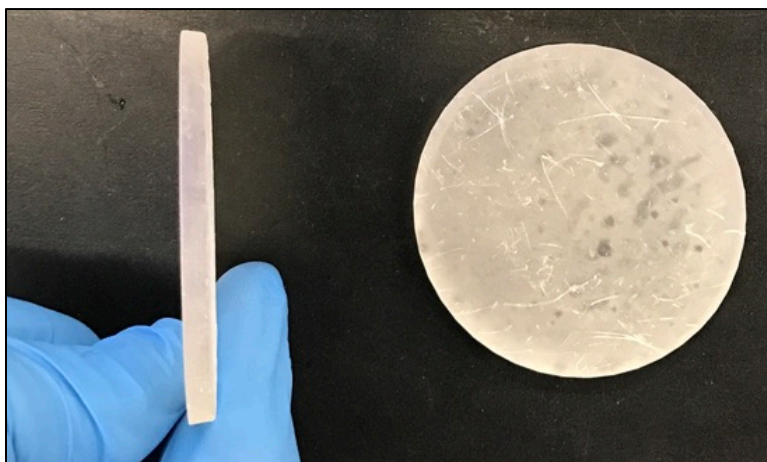
Figure 28. Disks printed with High Temp Resin for chemical resistance tests.

Disks were then submerged in solutions typically encountered during the biodiesel transesterification reaction, including 0.6M NaOH in water, 1M NaOH in water, 0.6M NaOH in methanol, and pure methanol. The disks remained submerged at 60˚C for seven days. During this

time, in roughly 24 hour intervals, the disks were removed and washed with water. After patting dry, the disk weights and dimensions were measured with an analytical balance and micrometer, respectively, and the disks were returned to the solutions.

6.2.1 Chemical Resistance Results

After one day of submersion, disks printed in Clear resin had deteriorated significantly in both methanol and the methanol and NaOH solutions. Because of this, the clear resin was determined to be unfit for biodiesel production reactions.

No disks experienced significant change in dimensions over the course of the experiment. The results of the High Temp mass measurements are shown in Figure 29. The only disk that experienced significant change in mass was Disk 3, which was submerged in the Methanol and NaOH solution. It was noted that when this disk was removed from solution, the disk was hard and the surface appeared unaffected. However, upon washing with water, the disk surface became soft and tacky. Furthermore, as seen in Figure 29, the disk mass dropped significantly from the second to last measurement to the last measurement, between which the disk was left to air dry. These changes in mass were thus attributed to the washing step. Because no significant amount of water should be present during the biodiesel transesterification reaction, the resin was deemed sufficiently resistant to the expected chemical conditions involved in biodiesel production experiments. However, reinvestigation of chemical resistance to the methanol and NaOH solution using a washing step that does not involve water is recommended to ascertain that the resin is, in fact, sufficiently resistant to the solution.
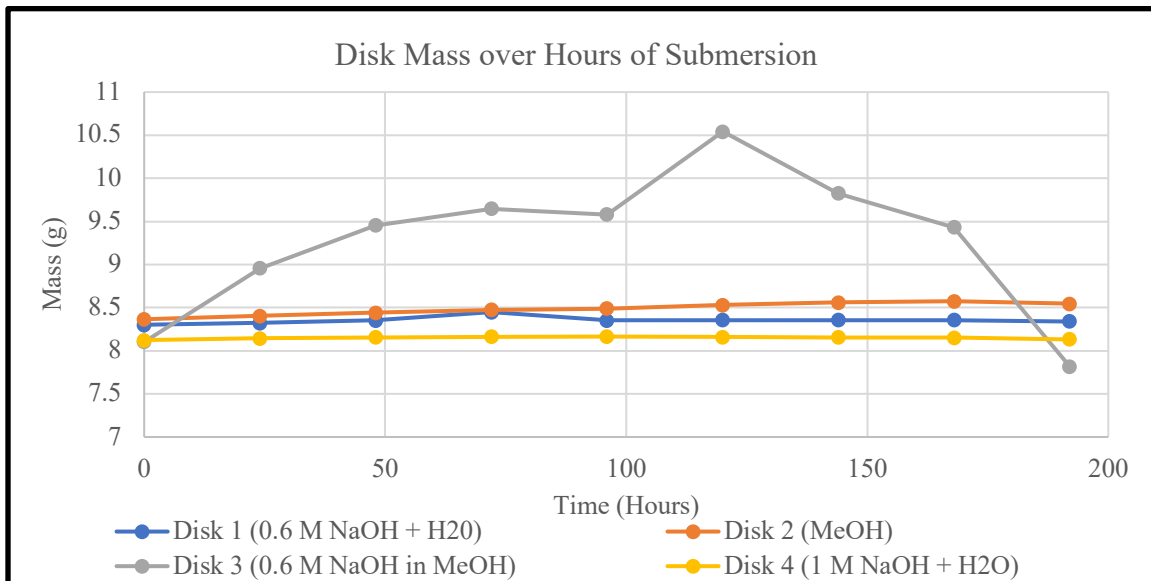
Figure 29. Chemical resistance results: Disk mass

6.3 Batch Biodiesel Experiment

A batch biodiesel production experiment based on an undergraduate laboratory handout was performed to serve as a point of comparison for future biodiesel production in microfluidic devices.[44] The experiment and results are detailed here.

6.3.1 Materials and Experimental Setup

60 mL of commercial, food-grade vegetable oil was measured and weighed. Then, a solution containing NaOH (at 1 weight percent of the oil) and 14 mL methanol was created. Both solutions were warmed to 60°C. They were then combined in a volumetric flask submerged in a water bath at 60°C. The reactants were then mixed for 30 minutes. After mixing, the products were transferred to a separatory funnel and allowed to settle (Figure 30).

Figure 30. Batch biodiesel experiment products before separation. Biodiesel is the top layer, while the bottom layer is mainly glycerin.

After settling, the bottom glycerin layer was drained and the biodiesel was slowly washed with

10 mL of deionized water. When the water settled, the biodiesel phase was collected for analysis.

6.3.2 Analysis and Results

The product was tested qualitatively using a 3:27 biodiesel test often used as a pass or fail

test for large scale home biodiesel production and in educational labs.[45] 3ml of the biodiesel was

combined with 27ml of methanol and shaken. The solution remained clear and no species settled

out of the solution, qualitatively indicating successful conversion to biodiesel. This simple

experiment served as a basis for comparison between batch and microfluidic production of

biodiesel, but was also intended to demonstrate a laboratory experiment that could easily be

performed in chemical engineering laboratory courses at UTC. Actual analysis of the product

following ASTM D6584-17 using gas chromatography methods is recommended for future

experiments to quantitatively and accurately determine extent of reaction.[46]

6.4 Biodiesel Production Experiments in 3D Printed Device

6.4.1 Materials and Experimental Setup

Modular fluid mixing devices, detailed in section 5.4, were printed, cured, and assembled

for use in biodiesel production experiments. The experimental setup is shown in Figure 31. 5 mL

of commercial vegetable oil was pulled into a syringe, and the mass of the oil was measured.

NaOH was measured out at 1 weight % of the oil and dissolved in 5ml of methanol. This

solution was also drawn into a syringe. Both reactant syringes were placed on the syringe pump.

The printed mixing device was submerged in a stirred hot water bath at 60˚C. The fluids were

pumped through the device at a rate of 2ml/hour and collected in a container submerged in a cold

water bath to terminate the biodiesel reaction. The products were allowed to settle, and the top

phase was removed and transferred to a new container by pipette and subsequently washed with

1ml of deionized water.
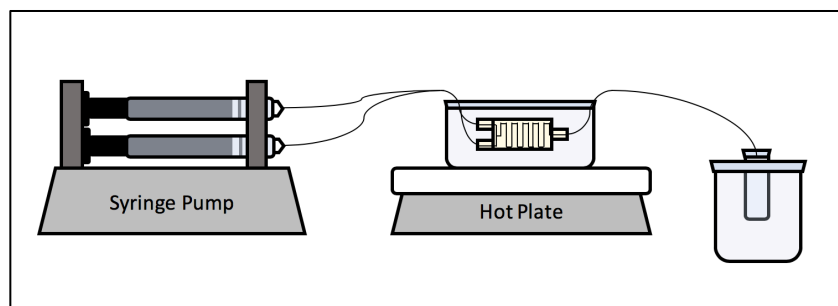
Figure 31. Setup for biodiesel production experiment. The syringe pump (left) feeds reactants into the mixing device which is submerged in a hot water bath (middle). Products are then collected in a vial submerged in a cold water bath (right).

6.4.2 Analysis and Results

During the experiment, bubbles and two phase flow were seen within the device

channels, indicating limited mixing of the reactants. Despite this fact, the resultant products

experienced color change compared to the reactants, indicating some extent of reaction (Figure 32). The bottom phase of the products did not appear dark as in the batch biodiesel production reaction, a phenomenon that should be explored more fully in the future. Upon washing with water, the products became cloudy, likely due to emulsification. The products were allowed to settle for 24 hours before separation.

Figure 32. Micro/millifluidic device biodiesel production experiment products (left) and pure vegetable oil (right).

After separation and washing, the resultant product passed the 3:27 test. Visual inspection of the device did not reveal degradation of the device over the course of the experiment. This experiment demonstrated the ability to conduct a biodiesel reaction inside a 3D printed micro/millifluidic device. Again, quantitative analysis of the products through gas chromatography or another method is recommended for future experimentation. As with mixing devices, it would also be beneficial to explore other device designs in addition to attempting to fabricate smaller channels which might encourage more efficient and complete mixing of fluids. Overall, this experiment serves as a basis for future exploration of biodiesel production in 3D printed micro and millifluidic devices.

CHAPTER 7: Droplet Generation

7.1 Overview

In this portion of study, water droplets in a continuous oil phase were created by use of a flow-focusing droplet generator. Droplets were generated at various oil to water flow rate ratios and the uniformity of resultant droplets was analyzed.

7.2 Device Design

The designed flow-focusing droplet generator (Figure 33) consisted of an entry port for oil, an entry port for water, and an exit port for oil and water droplets. The channels were designed such that the oil approached the water flow from two sides as to facilitate droplet break-off. The main middle cylindrical channel and the two cylindrical channels through which the oil approaches the main channel all had designed radii of 0.5 mm.
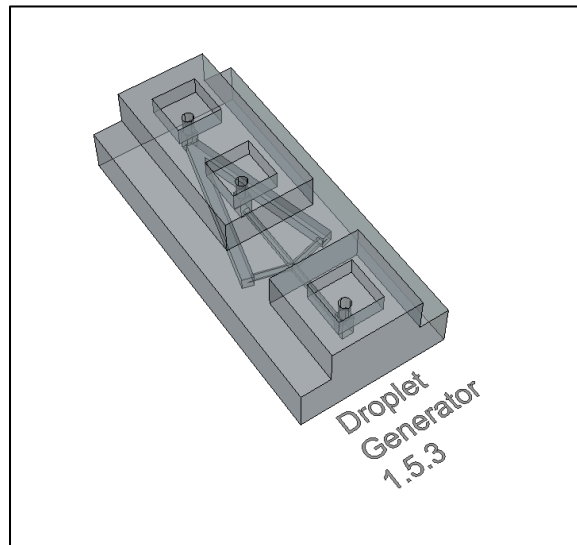
Figure 33. Model of droplet generator.

7.3 Droplet Generation Experimental Methods

Figure 34 shows a view of the internal channels of the printed droplet generator from the bottom of the device.
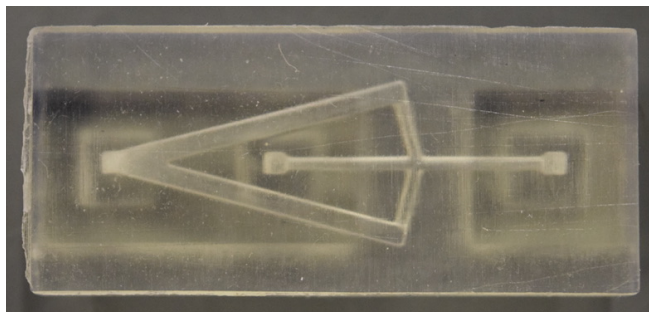
Figure 34. Droplet generator channels viewed from bottom of device.

Droplets were generated with varied water to oil flow ratios, including 1:1, 1:2, and 1:2.8, by use of various sizes of syringes. Ideally, multiple syringe pumps would be used to manipulate flow rates, but only one syringe pump was available for this study. Water droplets were collected in vegetable oil on a microscope slide fitted with 3D printed sidewalls used to contain the oil. Resultant water droplets were imaged and measured using optical microscopy, after which droplet uniformity at varied flow ratios was analyzed.

7.4 Droplet Generation Results

The printed droplet generation device is pictured in use in Figure 35, and example of collected droplets for analysis is shown in Figure 36.
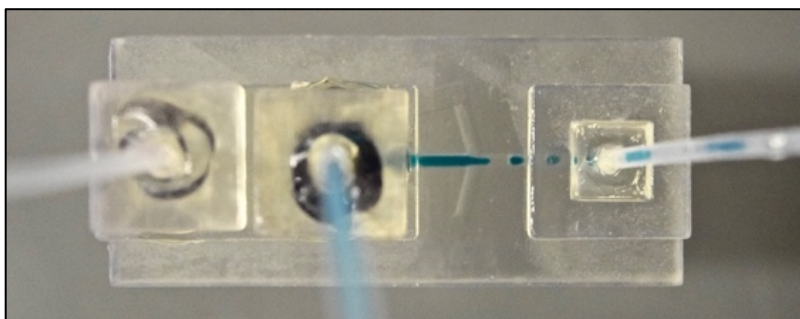
Figure 35. Printed droplet generator device during droplet generation experiment.
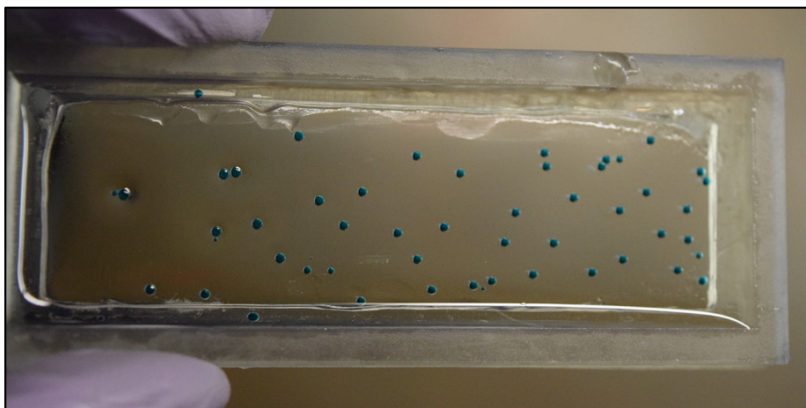
Figure 36. Water droplets in continuous oil phase in device created for droplet collection and analysis.

Droplet generation studies demonstrated successful production of various sizes of water droplets at different oil to water flow rate ratios. 20 droplets were analyzed for each flow ratio. At a 1:1 oil to water ratio the mean droplet radius was determined to be 597 ± 38.8 μm. Droplets produced at a 2:1 oil to water ratio were much more uniform with a mean radius of 451 ± 5.9 μm. Droplets generated at a 2.8:1 oil to water ratio were slightly less uniform with a mean radius of 455 ± 13.5 μm, and it is theorized that this variance was a result of inconsistent flow rate of both liquids due to lower quality syringes being used during that portion of the study. This study demonstrated the ability to tune water droplet size in the printed device through varying the oil to water flow ratio, and this technology may be applied to coursework in chemical and biomolecular engineering, as well as research projects involving biomimetic membranes.[47,48] Future work on droplet generators may also look to create other droplet generator designs in which droplet size may be influenced by active methods, such as manual control of orifice size where the oil and water meet.

CHPATER 8: Conclusion

8.1. Conclusion

This work demonstrated the ability to directly print micro and millifluidic devices for use in undergraduate engineering courses and research using a commercial SLA 3D printer and photopolymer resin. Laminar flow and fluid mixing were first shown in two different printed devices, one of which demonstrated physical modular connection of multiple devices. Other devices which did not successfully demonstrate fluid mixing may serve as a basis for future exploration of fluid mixing in 3D printed devices. After this, a similar mixing device was used during a biodiesel production experiment, the products of which passed a common qualitative biodiesel test. Finally, a droplet generator was printed and used to generate various sizes of water droplets in a continuous oil phase. Every one of these devices could be applied in some area of undergraduate study at UTC, including standard engineering courses or research. Overall, this study successfully demonstrated proof-of-concept for the use of SLA 3D printing for the production of micro and millifluidic devices intended for fluid mixing, biodiesel production, and droplet generation studies at UTC and beyond.

8.2 Future Work

Future work will focus on improvement of 3D printing device fabrication, the evaluation of 3D-printed micro and millifluidic device use for other applications, and integration of these devices into courses and research at UTC. In terms of improvement of 3D printing device fabrication, the largest challenge to address is achieving the ability to directly print smaller viable and flushable internal channels. Every portion of this study was affected by the inability to print smaller channels using the printing methods employed, and gaining the ability to print

channels could increase the effectiveness and expand the possible applications of these devices. A variety of other applications for these devices exist at UTC, including the encapsulation of cells, the processing of nanoparticles, and other types of chemical synthesis.

In terms of education, videos depicting laminar flow, diffusive mixing, and droplet generation may be created for use in engineering lecture courses. Hands-on experiments could also be developed to complement this lecture material in associated laboratory courses. Feasible target courses include: fluid mechanics and fluid mechanics laboratory, chemical process principles and unit operations laboratory, and chemical process operations and chemical processes laboratory. Current researchers at UTC in bioengineering may also seek to incorporate this technology into undergraduate research projects. By creating hands-on experiments involving these 3D printed devices, UTC student success, confidence, and retention could be positively impacted.

REFERENCES

1. Kaltschmitt, M.; Themelis, N. J.; Bronicki, L. Y.; Soder, L.; Vega, L. A., Renewable Energy Systems. SPRINGER VERLAG GMBH: 2013.
2. Rahimi, M.; Aghel, B.; Alitabar, M.; Sepahvand, A.; Ghasempour, H. R., Optimization of biodiesel production from soybean oil in a microreactor. Energy Conversion and Management 2014, 79, 599-605.
3. Kegley, B. J. D. The effect of co-solvent and ordered lattice structure on catalysis of biodiesel production in microreactors. University of Tennessee at Chattanooga, 2014.
4. Schmal, M., Heterogeneous Catalysis and its Industrial Applications. Springer International Publishing: 2016.
5. Rodenbusch, S. E.; Hernandez, P. R.; Simmons, S. L.; Dolan, E. L.; Knight, J., Early Engagement in Course-Based Research Increases Graduation Rates and Completion of Science, Engineering, and Mathematics Degrees. 2016, 15 (2), ar20.
6. National Academies of Sciences, E.; Medicine, Undergraduate Research Experiences for STEM Students: Successes, Challenges, and Opportunities. The National Academies Press: Washington, DC, 2017; p 278.
7. Carisa, H. R. P. E.; John, J. P. P. E., Improving Retention of Student Understanding by Use of Hands-on Experiments in Statics. ASEE Conferences: Indianapolis, Indiana.
8. Sarah Ilkhanipour, R.; Peter, A. S.; Zachary Aaron, S.; Wade Gerald, S.; Kevin, R. G.; Jason, G., Connecting Theoretical Concepts to Physical Phenomena Using 3-D-printed Microfluidic Devices. ASEE Conferences: Salt Lake City, Utah.
9. Brenda, R.-D., Hands-on Activities to Improve Students' Conceptual Understanding of Water Hardness. ASEE Conferences: Salt Lake City, Utah.
10. Freeman, S.; Eddy, S. L.; McDonough, M.; Smith, M. K.; Okoroafor, N.; Jordt, H.; Wenderoth, M. P., Active learning increases student performance in science, engineering, and mathematics. 2014, 111 (23), 8410-8415.
11. Beauchamp, M. J.; Nordin, G. P.; Woolley, A. T., Moving from millifluidic to truly microfluidic sub-100-μm cross-section 3D printed devices. Analytical and bioanalytical chemistry 2017, 409 (18), 4311-4319.
12. Esfahani, M. M. N.; Tarn, M. D.; Choudhury, T. A.; Hewitt, L. C.; Mayo, A. J.; Rubin, T. A.; Waller, M. R.; Christensen, M. G.; Dawson, A.; Pamme, N., Lab-on-a-chip workshop activities for secondary school students. Biomicrofluidics 2016, 10 (1), 011301-011301.
13. Mason, B. P.; Price, K. E.; Steinbacher, J. L.; Bogdan, A. R.; McQuade, D. T., Greener Approaches to Organic Synthesis Using Microreactor Technology. *Chemical Reviews* 2007, *107* (6), 2300-2318.
14. Guckenberger, D. J.; de Groot, T. E.; Wan, A. M. D.; Beebe, D. J.; Young, E. W. K., Micromilling: A method for ultra-rapid prototyping of plastic microfluidic devices. Lab on a chip 2015, 15 (11), 2364-2378.
15. Gale, B.; Jafek, A.; Lambert, C.; Goenner, B.; Moghimifam, H.; Nze, U.; Kamarapu, S., A Review of Current Methods in Microfluidic Device Fabrication and Future Commercialization Prospects. 2018, 3 (3), 60.
16. Dietzel, A., Microsystems for Pharmatechnology: Manipulation of Fluids, Particles, Droplets, and Cells. Springer International Publishing: 2016.
17. Waheed, S.; Cabot, J. M.; Macdonald, N. P.; Lewis, T.; Guijt, R. M.; Paull, B.; Breadmore, M. C., 3D printed microfluidic devices: enablers and barriers. *Lab on a Chip* 2016, *16* (11), 1993-2013.
18. Morgan, A. J. L.; Hidalgo San Jose, L.; Jamieson, W. D.; Wymant, J. M.; Song, B.; Stephens, P.; Barrow, D. A.; Castell, O. K., Simple and Versatile 3D Printed Microfluidics Using Fused Filament Fabrication. PLOS ONE 2016, 11 (4), e0152023.
19. Dragone, V.; Sans, V.; Rosnes, M. H.; Kitson, P. J.; Cronin, L., 3D-printed devices for continuous-flow organic chemistry. Beilstein Journal of Organic Chemistry 2013, 9, 951-959.
20. Tsuda, S.; Jaffery, H.; Doran, D.; Hezwani, M.; Robbins, P. J.; Yoshida, M.; Cronin, L., Customizable 3D Printed 'Plug and Play' Millifluidic Devices for Programmable Fluidics. PLOS ONE 2015, 10 (11), e0141640.
21. The Ultimate Guide to Stereolithography (SLA) 3D Printing. https://formlabs.com/blog/ultimate-guide-to-stereolithography-sla-3d-printing/ (accessed November 10, 2018).
22. Squires, T. M.; Quake, S. R., Microfluidics: Fluid physics at the nanoliter scale. Reviews of Modern Physics 2005, 77 (3), 977-1026.
23. Minnella, W. Microfluidics and Its Aplications: A Short Review 2013. https://www.elveflow.com/microfluidic-tutorials/cell-biology-imaging-reviews-and-tutorials/microfluidic-for-cell-biology/microfluidics-applications-a-short-review/ (accessed November 10, 2018).

24. Ward, K.; Fan, Z. H., Mixing in microfluidic devices and enhancement methods. Journal of micromechanics and microengineering : structures, devices, and systems 2015, 25 (9), 094001.

25. Kuo, J. S.; Chiu, D. T., Controlling mass transport in microfluidic devices. Annual review of analytical chemistry (Palo Alto, Calif.) 2011, 4, 275-296.

26. Lee, C.-Y.; Wang, W.-T.; Liu, C.-C.; Fu, L.-M., Passive mixers in microfluidic systems: A review. Chemical Engineering Journal 2016, 288, 146-160.

27. Cai, G.; Xue, L.; Zhang, H.; Lin, J., A Review on Micromixers. 2017, 8 (9), 274.

28. Kiss, A. A., Process intensification technologies for biodiesel production: reactive separate processes. Springer: Cham:, 2014.

29. Littell, M. Effect of a co-solvent feedstock on the synthesis of biodiesel via heterogeneous catalysis. The University of Tennessee at Chattanooga, 2015.

30. Billo, R. E.; Oliver, C. R.; Charoenwat, R.; Dennis, B. H.; Wilson, P. A.; Priest, J. W.; Beardsley, H., A cellular manufacturing process for a full-scale biodiesel microreactor. Journal of Manufacturing Systems 2015, 37, Part 1, 409-416.

31. Bardin, D.; Lee, A. P., Low-cost experimentation for the study of droplet microfluidics. Lab on a chip 2014, 14 (20), 3978-3986.

32. Morgan, A. J. L.; Hidalgo San Jose, L.; Jamieson, W. D.; Wymant, J. M.; Song, B.; Stephens, P.; Barrow, D. A.; Castell, O. K., Simple and Versatile 3D Printed Microfluidics Using Fused Filament Fabrication. PloS one 2016, 11 (4), e0152023-e0152023.

33. Gu, H.; Duits, M. H. G.; Mugele, F., Droplets formation and merging in two-phase flow microfluidics. International journal of molecular sciences 2011, 12 (4), 2572-2597.

34. Yeh, C.-H.; Chen, Y.-C.; Lin, Y.-C., Generation of droplets with different concentrations using gradient-microfluidic droplet generator. Microfluidics and Nanofluidics 2011, 11 (3), 245-253.

35. Form 1+: Introducing Desktop SLA. https://formlabs.com/media/upload/Form-1-plus-overview-US.pdf.

36. Gu, H.; Duits, M. H. G.; Mugele, F., Droplets Formation and Merging in Two-Phase Flow Microfluidics. 2011, 12 (4), 2572.

37. Form 2. https://formlabs.com/store/us/form-2/ (accessed November 10, 2018).

38. The Future of the Form 1+. https://forum.formlabs.com/t/the-future-of-the-form-1/12347 (accessed November 10, 2018)

39. Materials Data Sheet: Photopolymer Resin for Form1+ and Form 2. https://formlabs.com/media/upload/XL-DataSheet.pdf (accessed November 10, 2018). Materials Data Sheet: Photopolymer Resin for Form1+ and Form 2. https://formlabs.com/media/upload/XL-DataSheet.pdf (accessed November 10, 2018).

40. Material Data Sheet: Standard. https://formlabs.com/media/upload/Clear-DataSheet.pdf (accessed November 10, 2018).

41. Alam, A.; Kim, K.-Y., Mixing performance of a planar micromixer with circular chambers and crossing constriction channels. 2013; Vol. 176, p 639–652.

42. Aubin, J.; Ferrando, M.; Jiricny, V., Current methods for characterising mixing and flow in microchannels. Chemical Engineering Science 2010, 65 (6), 2065-2093.

43. ASTM D543-14, Standard Practices for Evaluating the Resistance of Plastics to Chemical Reagents, ASTM International, West Conshohocken, PA, 2014, www.astm.org

44. Katz, D., The Synthesis of Biodiesel from Vegetable Oil. 2012.

45. Gross, E. M.; Williams, S. H.; Williams, E.; Dobberpuhl, D. A.; Fujita, J., Synthesis and Characterization of Biodiesel from Used Cooking Oil: A Problem-Based Green Chemistry Laboratory Experiment. In Green Chemistry Experiments in Undergraduate Laboratories, American Chemical Society: 2016; Vol. 1233, pp 71-92.

46. ASTM D6584-17, Standard Test Method for Determination of Total Monoglycerides, Total Diglycerides, Total Triglycerides, and Free and Total Glycerin in B-100 Biodiesel Methyl Esters by Gas Chromatography, ASTM International, West Conshohocken, PA, 2017.

47. Jang, M.; Yang, S.; Kim, P., Microdroplet-based cell culture models and their application. BioChip Journal 2016, 10 (4), 310-317.

48. Taylor, G.; Nguyen, M.-A.; Koner, S.; Freeman, E.; Collier, C. P.; Sarles, S. A., Electrophysiological interrogation of asymmetric droplet interface bilayers reveals surface-bound alamethicin induces lipid flip-flop. Biochimica et Biophysica Acta (BBA) - Biomembranes 2018